https://doi.org/10.1016/j.jece.2023.110550

Multilayer Graphene Oxide-based Membranes for Reverse Osmosis Water Desalination: an Atomistically Detailed Simulation Study

K. Karatasos[1,*], G. S. Fanourgakis[2], I. Zuburtikudis[3] and Hadil Abu Khalifeh[3]

1.Chemical Engineering Department, Aristotle University of Thessaloniki, 54124 Thessaloniki, Greece

2.Chemistry Department, University of Thessaloniki, 54124 Thessaloniki, Greece

3.Chemical Engineering Department, Abu Dhabi University, P.O. Box 59911, Abu Dhabi, U.A.E

Abstract

Pressure-driven Molecular Dynamics simulations were employed to examine reverse osmosis desalination through graphene-oxide-based multilayered membranes. The effects of functionalization of the graphene-oxide flakes with poly(ethylene imine) branches in water permeability and salt rejection were described in detail. The role of the degree of structural rigidity of the membranes was also explored. A lower degree of rigidity of the membrane resulted in a 6% to 9% increase in water permeability depending on the state of functionalization of the flakes. At constant membrane rigidity, functionalization of the membranes' flakes led to approximately 30% reduction in water permeability, but the water flux remained 2-3 orders of magnitude higher than that of conventional reverse-osmosis membranes. Moreover, functionalization of the membranes' flakes resulted in a higher than 20% enhancement in salt rejection at a pressure difference similar to that in actual reverse osmosis processes. Examination of the swelling behavior of the membranes showed that those based on the functionalized flakes exhibit a tendency to remain structurally coherent with an interlayer separation determined by the presence of the polymer branches. Description of the microscopic mechanisms related to the membranes' water and ion flux, such as hydrogen bonding and concentration polarization, allowed the assessment of the contribution of different factors involved in desalination, providing new insight towards the fabrication of membranes with improved performance.

Keywords: Non-Equilibrium Molecular Dynamics, Multilayered Membranes, Functionalized Graphene Oxide, Poly(ethyleneimine), Reverse Osmosis, Desalination.

*Corresponding author: E-mail: kkaratas@cheng.auth.gr (K. Karatasos)

1.Introduction

One of the most promising methods to alleviate the fresh water shortage is desalination [1], as it can provide a sustainable water supply beyond the resources offered by the hydrological cycle[2]. Conventional water treatment technologies require significant energy consumption while performing in suboptimal levels in removing salt ions or other volatile organic pollutants[3, 4]. Among different water treatment methods, membrane-based filtration processes can play a crucial role in water purification and desalination, since they are energy efficient, easy to implement and are based on environmentally friendly operating conditions[5]. Particularly for desalination purposes, carbon compounds such as graphene and its derivatives, have emerged as promising materials for the fabrication of nanocomposite membranes[6-9]. The development of efficient synthetic protocols for their large-scale production[10] and the ability of such compounds to improve key membrane properties such as their mechanical strength, thermal stability and chemical inertness[11, 12] have placed them under the focus of the scientific and the industrial community.

In this context, several nanofiltration membranes constructed by oxidized forms of graphene, i.e., graphene oxide (GO), have been reported to exhibit improved performance in ion separation and molecular sieving processes[13-17]. GO flakes are layered oxygenated graphene sheets, containing oxygen functional groups such as epoxides, carboxyls and hydroxyls on their basal planes and edges, rendering them water soluble. Although significant progress has been achieved in the efficiency of GO-based membranes in nanofiltration, reverse osmosis and electrodialysis processes, there is still need for improving the membranes' design, towards higher water permeability, higher ionic selectivity and more stable performance[18, 19].

One way to meet such requirements is by exploiting the versatility of GO to be chemically functionalized in a desired manner[20-22]. The efficiency of GO membranes in terms of selectivity and/or water permeability can be improved by modifying the GO oxidation pattern or by properly spacing and bonding the GO nanosheets through the intervention of different-sized linkers, or separators[15, 16, 23-26]. Functionalization of the GO sheets with dendritic and hyperbranched polymers may serve this purpose[27-30] by providing a better control of the separation between adjacent GO sheets, resulting in a fine-tuning of the sieving performance through size exclusion. Furthermore, it may improve ion selectivity and adsorption, due to ability of certain dendritic

functional groups to assume different ionization states upon proper variation of the solution pH [31, 32], thus enabling the regulation of electrostatic interactions between the ions and the GO flakes.

A rational route for improving the design of the Graphene-based membranes is to acquire a detailed understanding of the microscopic mechanisms which are responsible for their permselectivity performance. To this end, molecular simulations may serve as an atomic-resolution tool, which can probe the elementary processes involved in these phenomena and shed light on the relative contribution of each parameter to the membrane's performance. This atomic-level information may complement relevant experimental studies, offering a better interpretation of the observed behavior and providing predictive capabilities towards a tailored design of membranes with optimized properties[33-35].

Molecular Dynamics (MD) simulation studies have demonstrated that single-layered porous graphene can be of great potential in seawater desalination and drinking water production[36, 37]. However, these types of membranes are difficult to fabricate since they are made by a single layer of graphene. Thus, despite the encouraging results from early computational studies, manufacturing of cost effective and structurally stable graphene-based membranes with the desired permselectivity is challenging[2, 38]. To address this issue, the use of multilayered GO-based membranes has been proposed. Fabrication of such membranes has become feasible using vacuum/pressure-assisted methods[39, 40], casting/coating-based processes[41, 42] and layer-by-layer self-assembly deposition techniques[43]. Significant progress in relevant experimental protocols resulted in multilayered GO membranes with enhanced stability, increased mechanical strength and improved anti-fouling properties, while continuous efforts towards their scalable and cost-effective production are currently in progress[2, 44, 45].

Valuable insight towards the improvement of the design and the performance of multilayered GO membranes, has been provided by computer simulations[15, 26, 46-55]. Several of these computational efforts have focused on the study of water and ion flow through a multilayer graphene-derived membrane driven by a pressure gradient[15, 26, 47, 49-51, 56-58], mimicking reverse osmosis (RO) conditions. The great interest towards an optimal design of membranes for RO processes emanates from the fact that it is the state-of-the-art technique for the desalination of seawater and brackish water, due to its reliability, its relatively low cost, and its suitability at areas where water availability is limited[2, 59, 60].

The present study aims at elucidating the pressure-induced ion rejection and water permeation effects related to the functionalization of multilayered GO-based membranes. Towards that goal, we have simulated a RO desalination process through a 3-layered membrane, comprised by GO flakes with or without the presence of chemically attached cationic poly(ethylenimine) (PEI) branches, at neutral pH conditions. Poly(ethyleneimine) is a water soluble and pH responsive polymer, which has already been used for the functionalization of graphene oxide[61], while membranes based on PEI-functionalized GO have recently been tested for water purification and separation processes[62-67].

The pressure differences applied ranged from 0 (i.e., with the absence of a pressure gradient) up to 1000bar. The lower pressure difference investigated under RO conditions (i.e., ~100bar), lies within the limits of the experimentally utilized pressures for RO operations [59]. In addition, by allowing different motional degrees of freedom of the GO flakes (either functionalized or not) during the simulations, we have assessed possible effects related to a moderate variability of the size of the nanochannels formed between the GO layers, during the desalination process.

2.Materials and Methods

2.1 *Description of the Systems*

The two variants of GO flakes used in the construction of the membranes and the structure of the branched PEI used for the functionalization of the GO sheets, are shown in figure 1.

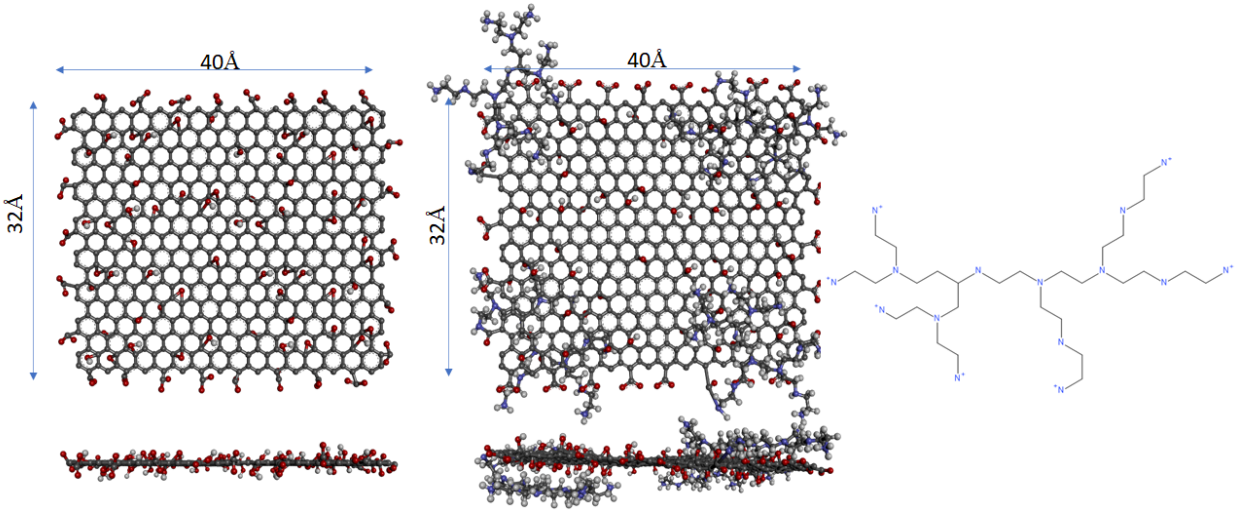

Figure 1. (Left) A non-functionalized, $C_{554}H_{36}O_{112}$, and (middle) a branched PEI-functionalized, $C_{666}H_{348}N_{60}O_{108}$, GO flake in frontal and lateral view. Carbon atoms are depicted in dark gray,

oxygen atoms in red, hydrogen atoms in white and nitrogen atoms in blue. A schematic of the branched PEI used for the functionalization of the GO nanosheets is shown at the rightmost part of the figure.

The GO flakes bear epoxide and hydroxyl groups placed randomly on both sides of the basal plane and peripheral carboxylate groups[68], in proportions commensurate to the Lerf-Klinowski model[69], with a carbon to oxygen ratio close to 5:1 and a hydroxyl to epoxy group ratio of 3:2 (with the carbons of the branched PEI in the functionalized flakes, not accounted for). The hydroxyl groups are not ionized, while the carboxylic groups are deprotonated, in order to simulate neutral pH conditions[70, 71]. Each functionalized GO flake bears 4 branched PEI molecules (of Mw~600Da)[72] attached to the peripheral carboxylate groups (see figure 1) according to previously reported chemical protocols[72, 73]. These are placed symmetrically on both sides of the surface to yield a balanced mass distribution. This functionalization scheme resulted in GO flakes with approximately 25wt% in PEI, which is within experimentally realizable proportions[72, 73].The branched PEI moieties are also partially protonated to simulate a neutral pH environment[32]. The protonation/deprotonation schemes adopted, resulted in a net charge for each non-functionalized flake of $-26|e^-|$ and for each functionalized one of $+1|e^-|$.

Two 3-layered GO membranes comprised by 10 flakes each were constructed, one comprised by the non-functionalized GO nanoflakes (GONF) and one comprised by the branched PEI-functionalized GO nanosheets (GOPEI), in a 4-2-4 configuration, as illustrated in figure 2.

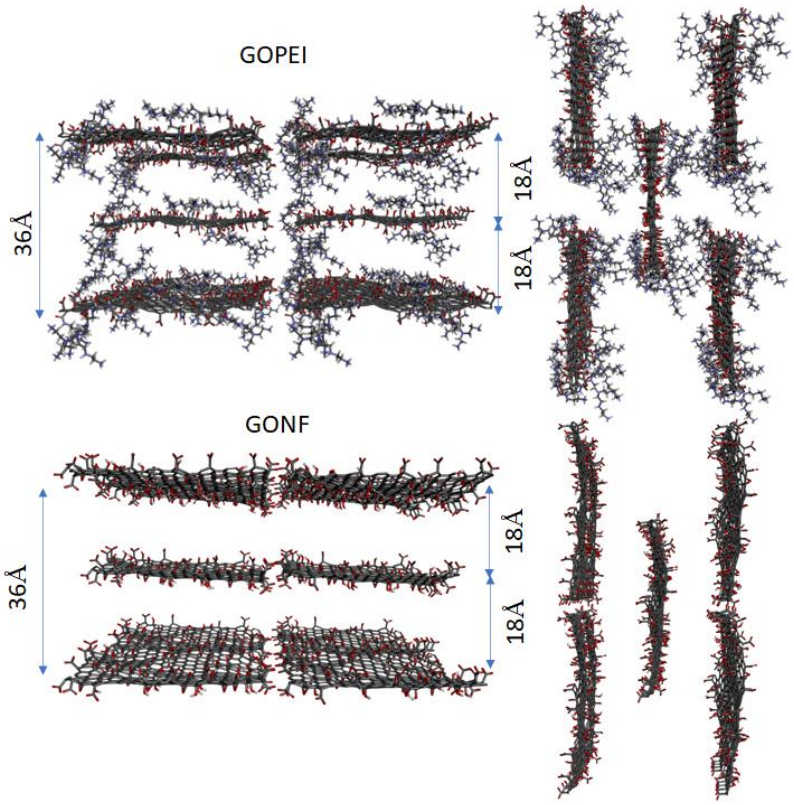

Figure 2. The 4(top layer)-2(middle layer)-4(bottom layer) configuration of the constructed membranes. The separation between the basal GO planes was constructed to be initially the same for both kinds of membranes. Water molecules used for the hydration of the membranes are omitted for clarity.

The placement of the 2 GO flakes in the intermediate layer serves as an aperture-reducing obstacle which creates an additional frictional force against the water transport through the membrane, mimicking more realistic flow conditions[74]. In addition, such overlapping flake arrangements are closer to experimental GO-based membrane structures[75-77], allowing the formation of water and ion diffusion paths, which may enhance the membrane's nanofiltration performance[6, 75]. In the system with the functionalized GO, the interlayer distance chosen was sufficient to accommodate the PEI branches; for comparison purposes the same distance was kept in the system comprised by the non-functionalized flakes. Although it was expected that a larger number of layers in the membrane's structure would result in a better performance in terms of ionic rejection[74], for computational efficiency purposes we opted in examining 10-flake membranes, adopting the 4-2-4 trilayer configuration described above. We mainly focused on the effects of the functionalization of the membrane's GO flakes with the PEI branched groups and the degree of

their mobility, while keeping constant other parameters such as the oxidation pattern and the degree of functionalization of the flakes, their size and their interlayer distance.

The initial configuration of the simulated setup consisted of 3 compartments: (a) a feed reservoir containing an aqueous NaCl solution of a 0.5M concentration, which has also been adopted in previous works [47, 55] and is close to the average seawater NaCl concentration[78, 79] (b) the hydrated membrane with an appropriate number of counterions in order to preserve the overall electrical neutrality and (c) a permeate water reservoir. At the left side of the feed reservoir and the right side of the permeate, graphene surfaces have been used as pressure-applying pistons[55, 80]. The dimensions of the graphene surfaces were 95 Å×105 Å, defining the x-y dimensions of the simulation box, while the total length (z-size) of the 3-compartment system was approximately 190Å (the z-dimension of each compartment was approximately the same). The lateral dimensions of the trilayer GO arrangement were moderately smaller than the xy dimensions of the simulation box, in order to mimic the presence of water nanochannels between the periodic images of the membrane. The average distance between the edges of the flake layers and the sides of the box in the initial configuration, ranges between 15Å (outer layers) to 30Å (inner layer) in the x-direction and close to 15Å for all flakes in the y-direction. The size of these nanochannels was larger than the dimensions of the hydrated Na^+ and Cl^- ions[74]. To avoid interaction of the pistons with its closest neighbors in the pressure-applying coordinate (here the z-direction)[23], an extra vacuum space extending to 65 Å adjacent to each of the graphene surfaces (i.e. at the left side of the left graphene surface and at the right side of the right graphene surface, as depicted in figure 3) was added in this direction.

Table 1 provides a detailed description of the contents of each compartment. Figure 3 depicts the initial setup of the systems prior to the commencement of the non-equilibrium (NEMD) runs.

Table 1: Initial composition of the systems' compartments

Systems	Total number of GO flakes in a 4-2-4 configuration	Number of waters in the feed reservoir	Number of Cl- ions in the feed reservoir	Number of Na+ ions in the feed reservoir	Number of waters in the hydrated membrane	Number of counterions in the hydrated membrane	Number of waters in the permeate reservoir
GOPEI	10	20429	195	195	18635	10/Cl^-	20819

GONF	10	20429	195	195	19016	260/Na^+	20819

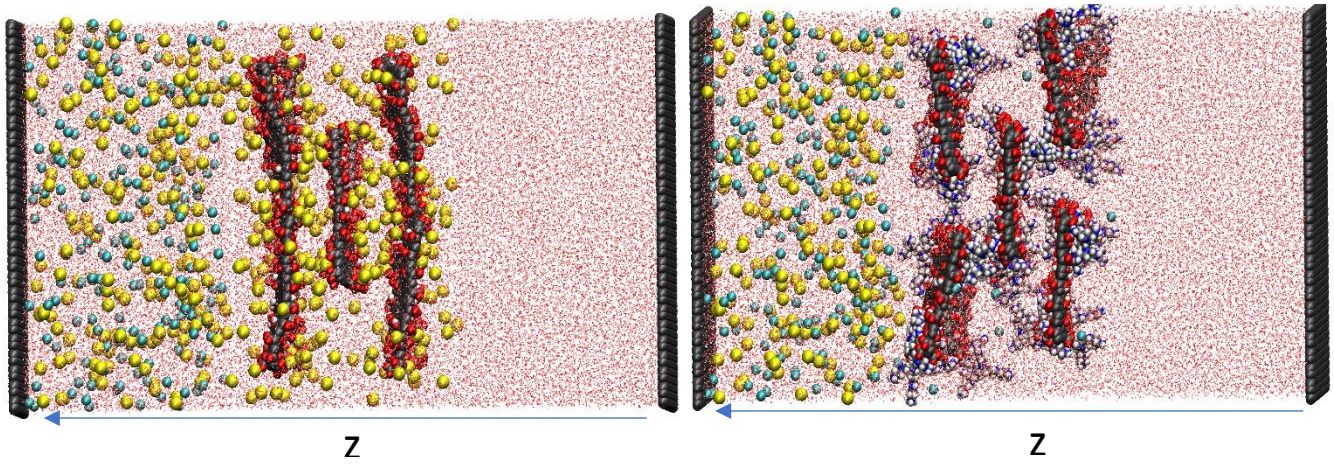

Figure 3: Initial setups of the GONF-based (left) and the GOPEI-based (right) simulated systems. Carbon atoms are shown in gray, oxygen atoms in red, hydrogen atoms in white, nitrogen atoms in blue, sodium atoms in yellow and chlorine atoms in dark cyan. Water atoms appear as red and white dots. The simulation box boundaries including the extra vacuum space is not shown. Arrows denote the direction of the positive z coordinate.

2.2 *Simulation Details*

All parameters used for the description of bonded and non-bonded interactions between the constituents of the examined systems, were taken from the OPLS-AA forcefield[81], which has previously been used for the parameterization of oxidized graphene forms[49, 82-85], of imine-based dendritic molecules[86] including ethyleneimine branched polymers[87], as well as for the energetic description of Na^+ and Cl^- ions[23, 49, 57, 88]. The rigid-body TIP3P model[89, 90] was utilized for the description of the water molecules. The TIP3P water model has previously been employed in combination with the OPLS-AA forcefield in GO aqueous dispersions[84] and RO simulations through GO nanochannels[23]. The carbon atoms of the graphene surfaces used for the application of pressure were modelled as electrically neutral generic aromatic carbons. Details on the types of atoms used according to the employed forcefield together with the corresponding partial charges and Lennard Jones parameters are provided in the supplementary material. Bonding information for our models are provided in separate files.

The initial state of the 3 compartments comprising each system, was prepared using the Packmol[91] and the VMD[92] packages. The atomistic MD simulations were performed by the

NAMD 2.14 program[93] using a cutoff of 12Å for the Van der Waals and real-space electrostatic interactions. The Particle Mesh Ewald (PME) method [94] was employed to account for the long-range electrostatic interactions. Periodic boundary conditions were applied in all directions.

The initial configuration of the combined 3-compartment system was constructed by a multistep procedure, which involved separate equilibration of each compartment. During the equilibration of each compartment an energy minimization procedure was followed by isochoric-isothermal (NVT) and isobaric-isothermal (NPT) MD runs at T=300K and P=1bar. Typical duration of the NPT runs for pressure/volume equilibration was of the order of 1ns. In the leftmost and the rightmost compartments, the graphene surfaces were kept fixed during the equilibration, while in the membrane-containing compartment (middle), the centers of mass of the GO flakes were also constrained. At the last stage, the energy of the combined system was minimized, and a short NPT MD run of about 50 ps was performed, in order to allow fine adjustments in the volume of the system. During this step, a very small percentage of water molecules may have exchanged places between the water reservoirs and the hydration layer of the membrane.

The so-constructed models were simulated in the NVT ensemble keeping the temperature constant at T=300 K, using a Nose-Hoover Langevin algorithm[95] with a decay time of 0.05ps. The timestep of the NVT simulations was 1fs and the frame-saving frequency was 5ps. The extent of the production trajectory depended on the system (i.e., functionlized or not), on the degree of mobility of the GO flakes of the membrane (i.e., fixed centers of mass or fixed edges) and on the applied pressure diffrence between the two pistons; the NEMD trajectory length varied from few ns to more than 125ns.

Application of pressure was implemented by adding an appropriate force to each atom of the graphene surfaces at every timestep in the direction of the compression (here the z-direction), by means of a home-developed script. The resulted force applied to each atom of the graphene pistons was calculated as $f=AP/n$ where A is the cross-section of the piston's surface, P is the desired pressure and n is the number of atoms in each graphene piston. In the graphene surface at the permeate reservoir, a constant pressure of 1 bar was always applied to mimic atmospheric conditions[57, 96]. In all simulations, the desired pressure applied to the graphene surface in the feed side remained constant during the simulation. We have performed simulations at feed pressures of 1bar, 100bar, 300bar, 500bar, 700bar and 1000bar. Although pressure differences higher than 100bar lie well above the range used in actual RO experiments[59], application of such

pressure gradients is a common practice in simulating RO processes[47, 49, 55, 80] in order to improve statistics and reduce thermal fluctuations at the timescales accessible at such simulations. The observed pressure-depended behavior can then be extrapolated to desired (lower) pressures, provided that appropriate scaling laws between the pressure gradient, the ion rejection and the water permeability are in order[26, 47, 74, 80].

In one set of the simulations the center of mass of each GO flake was constrained to its initial position by applying a harmonic potential to each one of them (denoted henceforth as fixed CMs systems). The force applied was therefore of the form f=-kr, where r denotes the distance between the center of mass of a flake at each instant and its position in the initial configuration, and k represents a spring constant which was taken to be 50 kcal/mol/Å. This value was found to be sufficient for maintaining the structural integrity of the membrane while allowing a rotational mobility of each GO flake around its center of mass, thus mimicking conditions where the membrane exhibits some degree of deformability. In another simulation set, the peripheral carbons of the carboxylate groups were kept fixed (referred to as fixed edges systems), reducing the motional degrees of freedom of the GO flakes and mimicking thus the response of a structurally rigid membrane. Therefore, for each pressure, 4 systems were simulated: 2 systems based on the GONF and 2 systems based on the GOPEI flakes (for each GO variant, one system with the centers of mass of the flakes fixed and one with the peripheral carboxylate carbon atoms of the flakes fixed). All simulations under non-vanishing pressure gradients were terminated at the time at which the feed reservoir became practically devoid of water.

3. Results and Discussion

3.1 *Water flux*

Water flow was monitored by tracking the variation of the number of water molecules in each compartment of the simulated systems during the simulation time. In all systems and under all pressure gradients applied, it was found that the number of the permeate water molecules increased, while those of the feed reservoir decreased linearly, at the same rate. On the other hand, the number of waters within the membrane remained stable during all simulations. Figure 4 depicts an example of this behavior at a feed pressure of 100bar and at the fixed CMs systems (Figure S1 in the supplementary material shows the behavior for the fixed edges systems).

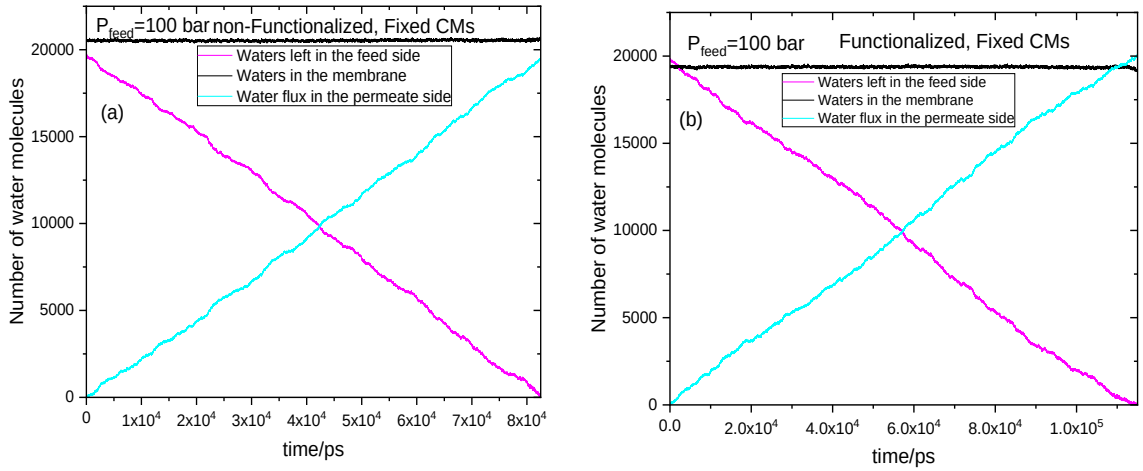

Figure 4: The number of waters in the feed reservoir, the net number of waters entering the permeate reservoir and the number of waters within the membrane as a function of time at a feed pressure of 100bar for the fixed CMs models with non-functionalized (a) and functionalized (b) systems.

Despite the similarities in water flow between the fixed CMs non-functionalized (figure 4a) and functionalized (figure 4b) systems, it is noteworthy that the timescale at which the feed reservoir becomes devoid of water molecules, is different. This is also the case when a similar comparison is made between the fixed edges systems (figure S1). An overview of this behavior is provided in figure 5, where the water fluxes from the feed reservoir are shown at different feed pressures, either referring to the same kind of flakes (Functionalized or non-Functionalized), or to the same kind of constraint imposed to the flakes (fixed CMs or fixed edges).

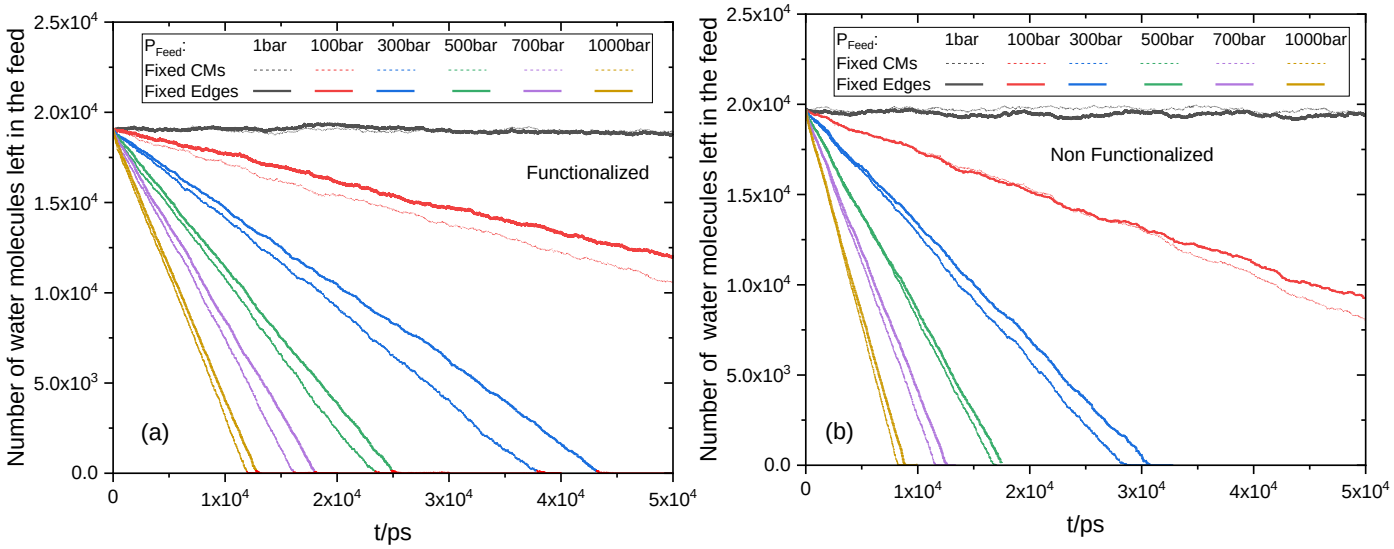

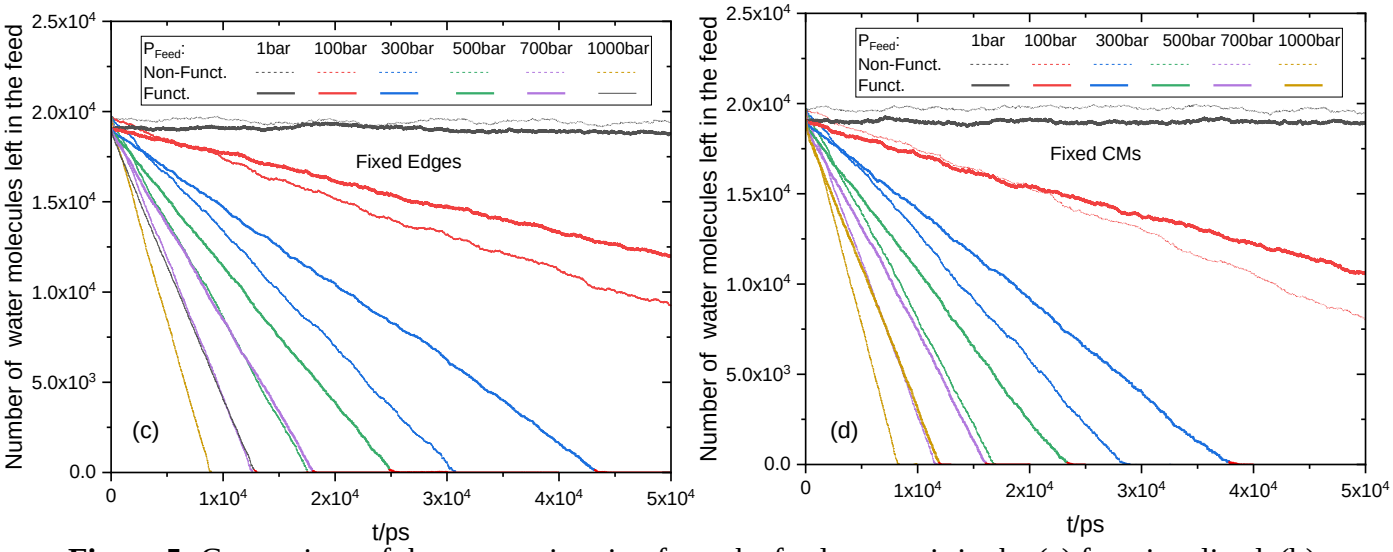

Figure 5: Comparison of the water migration from the feed reservoir in the (a) functionalized, (b) non-functionalized, (c) fixed edges and (d) fixed CMs models.

A visual inspection of the feed-water flow leads to some general conclusions: i) the timescale for the depletion of feed waters reduces, as expected, with the increase of the applied pressure gradient ii) this timescale is shorter for the fixed CMs systems, either functionalized (figure 5a) or not (figure 5b) iii) this timescale is longer for the functionalized models, either in systems with fixed edges (figure 5c) or with fixed CMs (figure 5d) iv) the effect of functionalization in increasing this timescale is considerably larger compared to that caused by fixing the edges of the flakes. The water flux from the feed reservoir to the membrane can be calculated at each pressure gradient by the slope of the respective curve. The flux from the membrane to the permeate has the same magnitude but opposite sign, since the net water flow in the membrane is always zero (see figures 4 and 5). The so-calculated water fluxes are plotted in figure 6, with respect to the pressure gradient applied in the pistons.

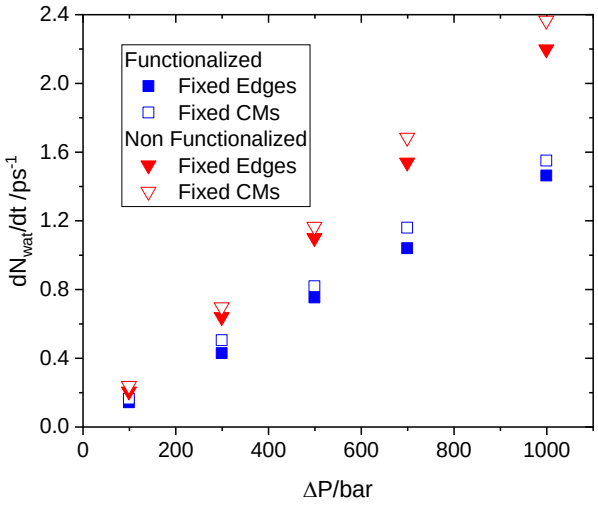

Figure 6: Water fluxes as a function of the applied pressure difference. Error bars are comparable in size or smaller to the size of the symbols.

In all cases, the rate of migration of water molecules from the feed to the membrane (or from the membrane to the permeate), varies linearly with the applied pressure difference, indicating steady hydraulic flow conditions. Comparison of the water fluxes between the functionalized and the non-functionalized models either for the fixed CMs or for the fixed-edges cases, shows that they deviate significantly at higher pressure differences, but appear to converge as the pressure gradient approaches the operational conditions of conventional RO processes. Comparison of the behavior between the fixed edges and the fixed CMs models (either for the GONF- or the GOPEI-based systems) shows that the fixed CMs models exhibit somewhat higher water fluxes. The respective water permeabilities were estimated from the slopes of the linear fits in figure 6, and are listed in Table 2.

Table 2: Water permeabilities for the simulated models in units of $Lm^{-2}h^{-1}bar^{-1}$ and $Lcm^{-2}day^{-1}MPa$ (in brackets).

	Fixed CMs	**Fixed Edges**
Non-Functionalized	2549±25 (61.2±0.6)	2397±16 (57.5±0.4)
Functionalized	1768±31 (42.4±0.7)	1605±21 (38.5±0.5)

The calculated water permeabilities are several orders of magnitude higher than those of conventional RO membranes[25, 97] or from those calculated for nonslip Poiseuille flows[26], but

comparable to the values estimated from computer simulations of pressure-driven water filtration through graphene-based membranes[15, 33, 36, 49].

The functionalized models exhibit between 33% (fixed edges) and 31% (fixed CMs) lower water permeabilities compared to their non-functionalized analogues. On the other hand, when fixed edges constraints are imposed, lower permeabilities between 6% (non-functionalized) and 9% (functionalized) compared to their fixed CMs counterparts are observed.

The reduction of water permeability associated with the kind of constraint imposed on the membrane's flakes observed in both, the functionalized and the non-functionalized models, should in principle be related to the different response of a fixed or of a mobile obstacle (here the GO flakes) which stands against water flow[98]. A previous computational study[51] examined the water permeability through a graphene-based multilayered membrane, comprised by flakes either with all their atoms fixed in space or with only the peripheral atoms fixed. It was concluded that the permeability in the models with the peripherally fixed atoms was higher; this behavior was attributed to the more efficient formation of nanochannels through which water molecules could diffuse within the membrane. In the absence of such nanochannels, as is the case in single-layered graphene membranes with pores, fixing the peripheral atoms of the flake resulted in a reduction of water permeability[99]. In this case, the observed behavior was attributed to the longer time needed for water molecules to cross a peripherally fixed membrane compared to the time required for crossing a completely fixed one.

A more quantitative manner to account for the behavior observed in our system with respect to the degrees of freedom of the GO flakes is to compare the potential of mean force (PMF) felt by the water molecules along the z-coordinate spanning the membrane. This can be calculated as $PMF(z) = -k_B T \ln [\rho(z)/\rho_0]$ [47, 57, 74] where k_B is the Boltzmann's constant, T the temperature, $\rho(z)$ the z-profile of water density, and ρ_0 is the density of water in the bulk (i.e., away from the membrane). Since this is a generic property of the membrane/water interaction, for better statistics we have calculated PMF(z) in the systems where no pressure gradient was applied (i.e., only when the osmotic pressure difference is present). Figure 7 portrays the so-calcuated PMF(z).

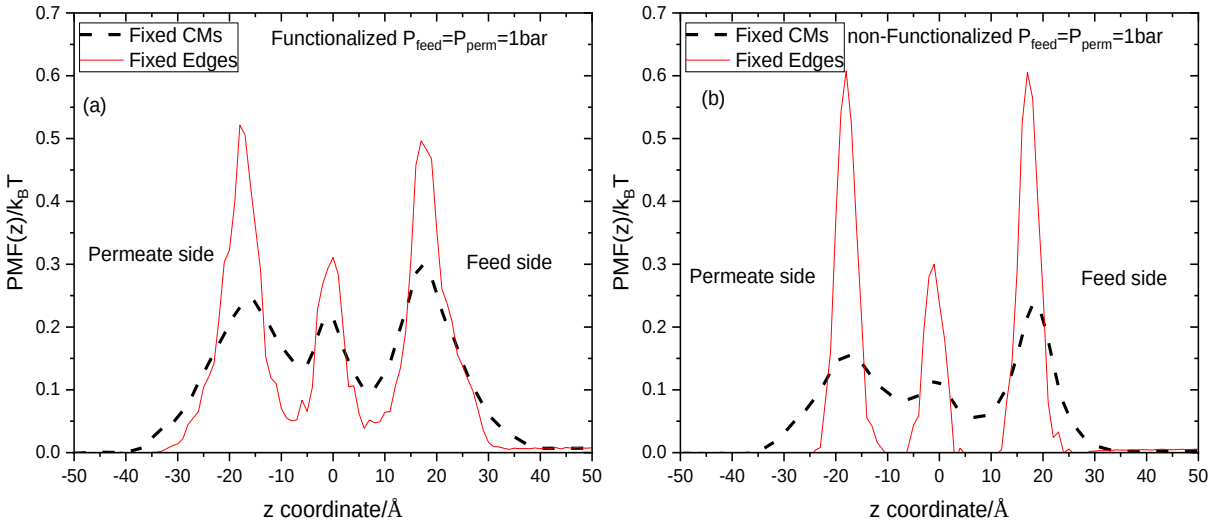

Figure 7: PMF(z) in units of k_BT for (a) the functionalized and (b) the non-functionalized models

The peaks in figure 7 denote the energetic barriers felt by water molecules across the membrane. The locations of the peaks correspond to the positions of the GO layers while the lower height of the middle peak is due to the fact that only two flakes are present in the intermediate layer, reflecting the 4-2-4 configuration of the membrane (see figures 2 and 3). For systems bearing either the functionalized or the non-functionalized flakes, the barriers are narrower and higher when the flakes are peripherally fixed, resembling a "resistance-in-series" model against water flow[47, 74]. This picture implies that water flux is expected to be lower in the fixed edges systems, as shown earlier. On the other hand, the area under the PMF(z) profiles, namely the reversible work needed for separating the water molecules from the membrane[100] was found to be larger in the functionalized systems, indicating a higher energetic affinity between the GOPEI-based membranes and water. Higher energetic affinities of membranes with waters, indicate lower water fluxes, in agreement with the results in Table 2.

To elaborate more on this point, since functionalization of the flakes is associated with the higher drop in water flux (see figure 6), we have examined the origin of the higher energetic affinity between water and the functionalized membrane, focusing more on hydrogen bonding interactions. This type of interaction is known to play a key role in the affinity between the water molecules and a GO-based membrane. Earlier studies have demonstrated the effect of hydrogen bonding on reducing water diffusion through GO layers[101] and showed the impact of the type of functionalization of the GO surface on the water/GO binding affinity[24, 25, 102, 103]. It was concluded that the hydrogen bonds formed between waters and functional groups of GO-based membranes were responsible for enhanced friction near the GO surfaces which contributed to the decrease of water flow [26, 46].

Counting of hydrogen bonds (Hbonds) in our systems was based on the following geometric criteria: (a) the distance between the donor and acceptor of the hydrogen should not exceed a defined cutoff distance, r_{cut}, and (b) the donor-hydrogen-acceptor angle should be less than θ_0 from 180°. Here r_{cut} was taken as 3.5Å and θ_0 as 30°[104]. Figure 8 shows the average number of Hbonds formed between the waters and the membrane, when either water molecules or GO flakes act as hydrogen bonding donors.

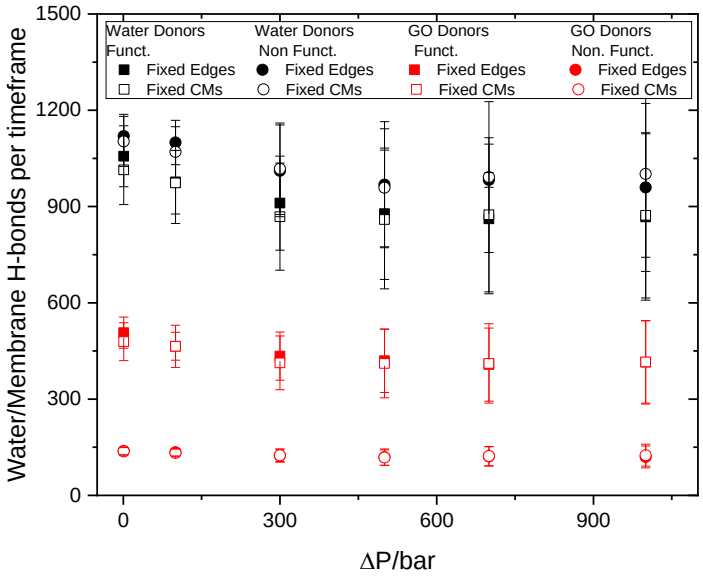

Figure 8: Hydrogen bonds formed between water molecules and GO flakes of the membrane as a function of the applied pressure gradient. Error bars denote standard deviations.

In all systems the average number of hydrogen bonds appears to be rather insensitive to the applied pressure gradient (ΔP), while the fluctuation of this number with respect to the average grows as ΔP increases. By counting only the hydrogen bonds in which water molecules act as donors and membranes' atoms as acceptors, no noticeable differentiation between the functionalized and the non-functionalized models is observed. However, by considering the case in which the GO flakes act as donors, an approximately 3-fold increase in the number of hydrogen bonds is seen in the functionalized membrane compared to the non-functionalized one. This difference should be ascribed to the fact that in the GONF flakes only the hydroxyl oxygens can serve as hydrogen bonding donors, while in the GOPEI models, nitrogen atoms of the branched PEI may serve as

donors, as well. Therefore, the higher number of hydrogen bonds between the waters and the functionalized membrane is consistent with the corresponding observed drop in the water flux.

3.2 *Ion Rejection*

The ability of the membranes to withhold the salt ions was examined by monitoring the number of ions passing through the membrane to the permeate. Figure 9 portrays the number of ions present in the permeate for the fixed CMs models, as a function of time. The behavior in the fixed edges models is shown in figure S2.

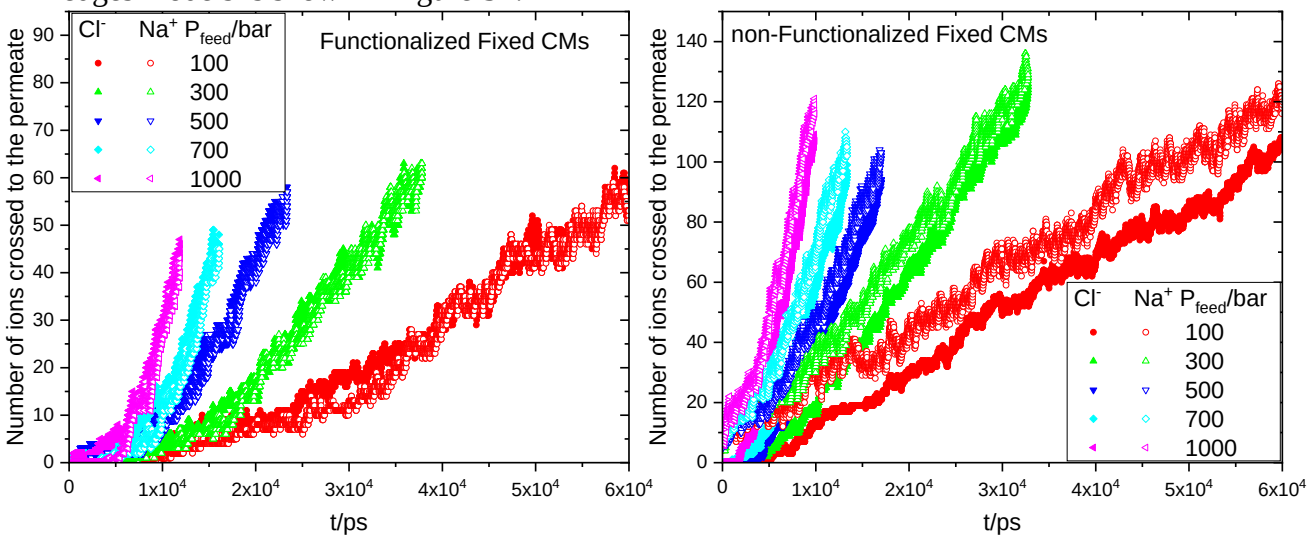

Figure 9: The number of salt ions present in the permeate as a function of time for the fixed CMs models

In both kinds of membranes, after a period of few ns during which a steady state is reached, the number of ions crossing to the permeate increases linearly with time. Upon increase of the net driving pressure applied to the pistons, the number of ions crossing to the permeate per unit time (as this is expressed by the slopes of the curves) increases as well. The rates of ion-crossing to the permeate are shown in figure 10.

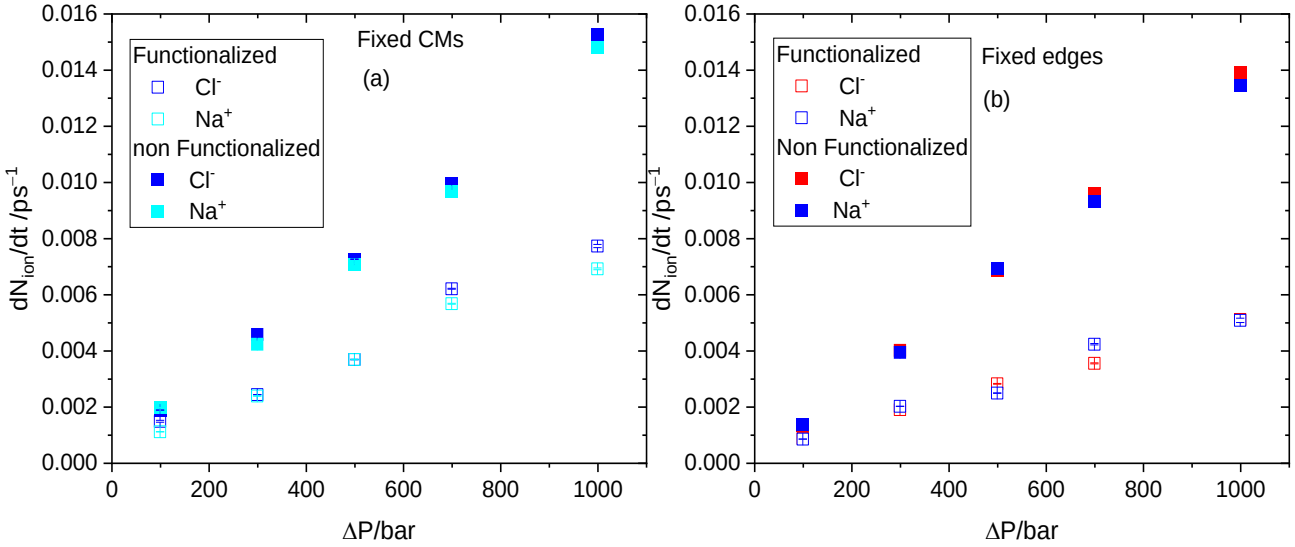

Figure 10: The rates (number of ions per unit time) of ion-crossing to the permeate as a function of the applied pressure difference for (a) the fixed CMs and (b) the fixed edges models. Error bars are comparable to the size of the symbols.

In all models, the rate of ion-crossing to the permeate increases linearly with the net applied pressure, ΔP. Irrespectively of the type of restriction imposed to the flakes, the rate of ion-crossing to the permeate per unit pressure difference (i.e., the slope of the linear dependence of the rate on ΔP), is lower when the membrane is comprised by functionalized flakes. At the same functionalization state, a slightly lower ion-crossing rate per unit pressure is observed only in the functionalized systems, when the flakes are peripherally fixed (see figure S3).

The above findings appear to imply on one hand that the functionalized membranes are more efficient in reducing the crossing rates of the ions per unit of net applied pressure, ΔP, and on the other hand that an increase in ΔP, will result in an increase of the ion flux towards the permeate. The latter is closely associated with the ion rejection performance of the membrane. However, since ion rejection must be calculated also in relation to the water flux towards the permeate, the pressure dependence of the ions rejection might not follow a simple linear law across the entire ΔP window[105]. In fact, if we compute the ratio of the ion fluxes over the corresponding water fluxes for our systems (see figure S4), it appears that this ratio does not vary linearly with ΔP over the entire pressure-window examined. Moreover, it appears that it assumes higher values at the lowest ΔP value examined here (i.e., ~ 100bar). To quantify this effect, we have calculated the ion rejection performance of the simulated membranes by estimating the fraction R of the rejected ions, as $R=1-N_t/N_0$; N_t denotes the number of ions present at the permeate side at a selected time t, while N_0 corresponds to the initial number of ions in the feed. The time *t* is usually defined in relation to a specific percentage of water that has been filtered. There have been several different values in the literature regarding the percentage of water that is considered for the definition of *t*,

such as ~10%[80], 20%[47, 57], 50%[47, 49, 57], 80%[15] depending on the system simulated. In our case we opted in taking *t* as the time at which 50% of water molecules have been transferred from the feed to the permeate side. This timescale corresponds to approximately half of the simulation time for each system (see figure 4), allowing for sufficiently accurate statistics under stable pressure-driven flow conditions. The dependence of this timescale on ΔP is linear for all the examined models (see figure S5).

Figure 11 shows the so-calculated ion rejection as a function of the applied pressure difference.

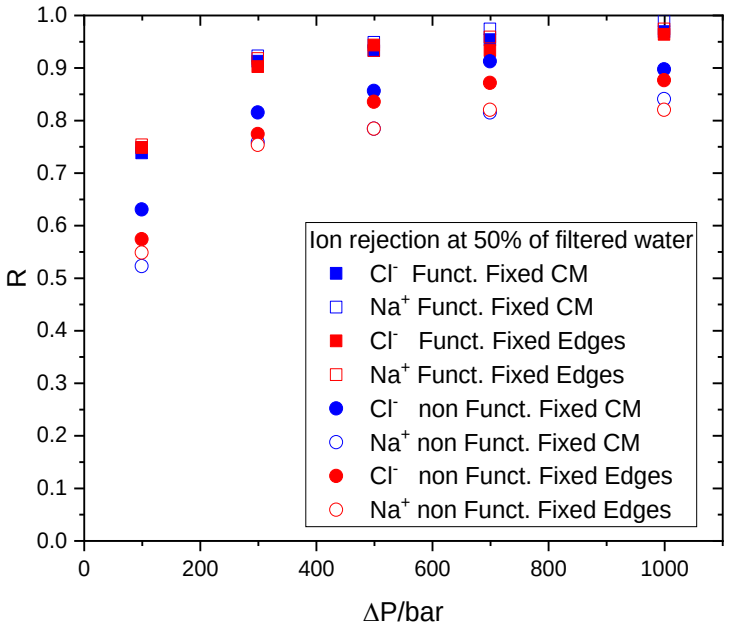

Figure 11: The fraction of rejected ions as a function of the applied pressure difference. The y-axis error margins are below 2%.

As a first remark, it appears that the functionalized models provide a 20% to 40% higher ion rejection compared to their non-functionalized analogues (particularly at lower pressure difference levels and depending on the type of ion examined). In the non-functionalized systems, a slightly lower degree of rejection is observed for the sodium ions. This could be related to the higher concentration of the sodium ions within the membrane, due to the presence of a large number of these ions initially placed in the membrane, to maintain its electrical neutrality. A higher concentration of these ions may induce an additional osmotic force towards the permeate and thus increase sightly their permeance. However, the presence of counterions initially placed to

neutralize the charge of the GO flakes, does not seem to affect the excess number of the respective counterions present within the membrane at any time, which is practically stable and similar between the two types of salt ions (see figure S1).

Another key feature present in all models is that the ion rejection appears to increase as the applied pressure difference increases. Since salt concentration in the permeate solution relates to the ratio of salt flux to water flux, and the increase in water flux with pressure is higher than the corresponding increase in salt flux (see fig. S4), it follows that the salt concentration in the permeate will drop with pressure (i.e., the rejection will increase). This observation comes into conflict with reports from previous computational works, where it was noted that an increase of the applied pressure gradient in general results in a decrease of ion rejection[47, 49, 57, 74, 105, 106]. However, in all the cases where ion rejection was reduced with the applied pressure gradient, the membranes examined were based on a single sheet or on a single pore, or on double-layered structures with a rather small separation (i.e., below 10Å) between them. In multilayered membrane structures, this effect was either diminished or completely vanished (with the rejection becoming independent of the applied pressure) when the number of layers became larger than two[74]. In other words, increase of ion rejection upon increase of the applied pressure difference, seems to be suppressed in cases where the membrane structure imposes a more complex path for ionic diffusion/advection, e.g., through the intervention of many layers, as is the case in our multilayered membranes.

Another key characteristic differentiating the present systems from the aforementioned works is that in our case the examined membranes were comprised by electrically charged flakes. Inclusion of permanent non-diffusible charges in the membrane enhances mechanisms such as the Donnan effect[107] or dielectric exclusion[108] due to the higher polarizability of the membrane, and influence the electromigration of the ions within its interior. Combination of these factors may induce concentration polarization (CP), i.e., an accumulation of charges in the membrane surface at the feed side, affecting thus the membrane's ion rejection capabilities[60, 109]. Although CP may lead to an undesirable decrease in water flux, in practice this can be mitigated by controlling the feed velocity or by other technical means[60]. On the other hand, this effect may result in an increase of the membrane's rejection performance upon increase of the applied pressure as has been experimentally observed [110, 111] and theoretically described [111, 112] in RO processes.

To check the development of CP during the simulation time in our systems, we have examined the z-coordinate number density distributions of the sodium and the chlorine ions. These distributions represent averages over the entire simulation time for each model. Figure 12 presents such distributions for the fixed CMs models. The distributions for the fixed edge models are shown in figure S6. Figure S7 shows an example of the ion number density profiles when averaged only over the initial 10ns and over the last 10ns of the trajectory. Visual inspection of the z-profiles in figure 12, shows an accumulation of both types of ions on the feed side of the membrane, indicating the development of CP. Actually, the area under the right-hand side "shoulder" of the profiles (i.e., that between the right boundary of the membrane and the point where the profiles reach zero) appears to increase as the pressure difference grows, indicating a CP enhancement with ΔP.

An enhanced CP is expected to result in an increased osmotic pressure at the membrane's surface, since osmotic pressure is proportional to salt concentration over a relatively wide range of salinities[113]. If we consider water permeability as an intrinsic membrane property which does not depend on feed concentration within the examined limits (as implied by figure 4), true ion rejection can be expressed as[114]

$R = \left(1 - \frac{\pi_{sl}}{\pi_{so(m)}}\right)$, where π_{sl} is the osmotic pressure in the permeate and $\pi_{so(m)}$ is the osmotic pressure at the membrane's surface. Therefore, an increase in $\pi_{so(m)}$ would result in an increase in R. This picture is consistent with a pressure-induced increase in ion rejection, in line with the trend observed in figure 11. An analogous behavior characterizes also the fixed edges models (figure S6) implying that this is a generic feature of both types of membranes.

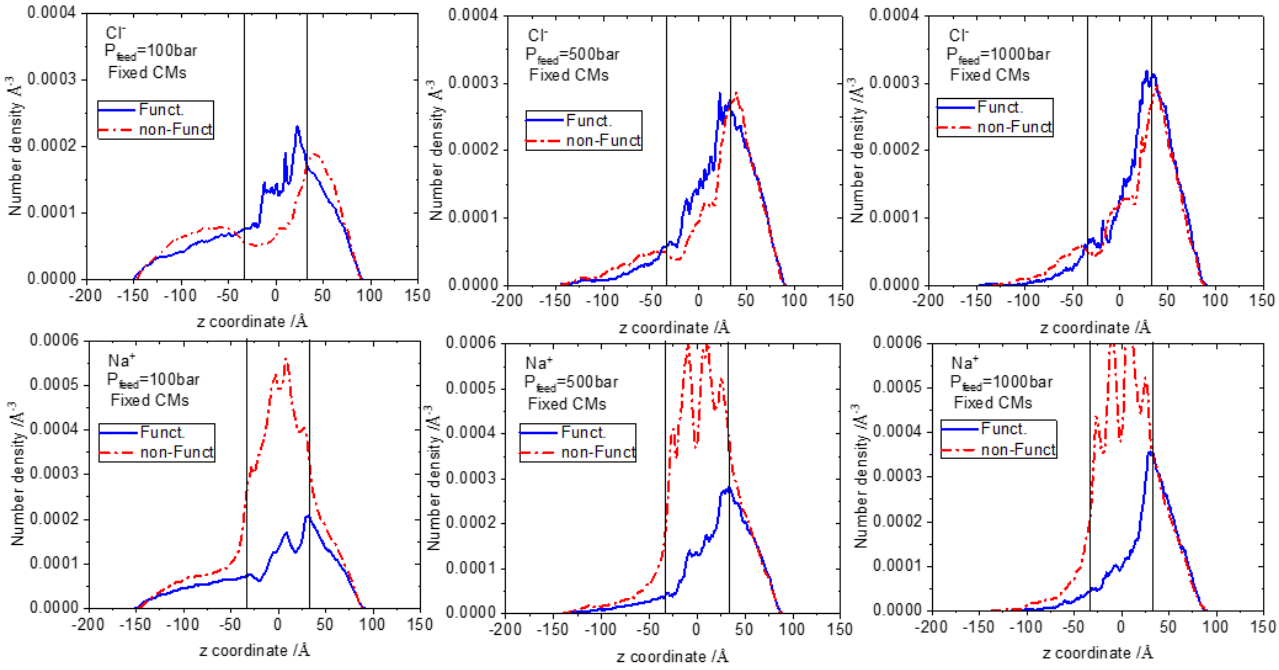

Figure 12: z-coordinate number density profiles for the chlorine (top row) and the sodium (bottom row) ions, at different feed pressures for the fixed CMs models. Vertical lines denote the boundaries of the membrane. The feed side lies on the positive values of the z coordinate.

To obtain more information regarding the relative affinity of the two types of ions with the membrane, while these are located within its limits, we estimated the van der Waals and the short-range electrostatic interactions between them. Although the contribution of the electrostatic forces from the periodic images of the simulation box were not taken into account, the contribution from the short-range electrostatics may offer a basis for discussion. These calculations are presented in figure S8. A general observation is that for all systems the main contribution in the ion/membrane interaction originates from electrostatic interactions. The level of spatial confinement imposed to the GO flakes does seem to affect the energetics between the membrane and the ions. However, the functionalization state of the flakes which changes the overall charge of the membrane, plays a crucial role. In the functionalized systems where the overall charge of the GO flakes is positive but relatively small (i.e., +10|e|), the electrostatic interaction between the membrane and the ions is attractive with a more favorable interaction between the flakes and the oppositely charged Chlorine ions. In the non-functionalized systems with the strongly charged flakes (i.e., bearing a total charge of -260|e|), the same sign ions, Cl^-, are effectively repulsed while the opposite-sign

ions are strongly attracted. These observations are consistent with a) the sharper peaks of the Cl^- density profiles within the membrane in the functionalized models (see figures 12 and S4) and b) the sharper peaks observed in the Na^+ profiles within the membrane in the non-functionalized models, since a sharp peak is indicative for a higher degree of localization of the ions close to the surface of the GO flakes. Particularly for the Na^+ ions, the sharp-peaked profiles are consistent with the formation of a layer of strongly adsorbed (i.e., condensed) ions onto the flakes' surface. Formation of such a layer would provide a more effective electrostatic screening of the GO flakes from the rest of the sodium ions, allowing them to cross to the permeate side under the effect of the remaining applied forces.

3.3. Swelling behavior of the membranes

To examine the swelling behavior of the membranes with the two different functionalization states of the flakes, we have performed simulations with the flakes unconstrained starting from an initial configuration corresponding to a fixed CM model and under zero pressure gradient conditions. We then monitored the change in the z-separation between the centers of mass of the flakes belonging to the intermediate layer and those belonging to the outer layers of the membrane (see Figure 13).

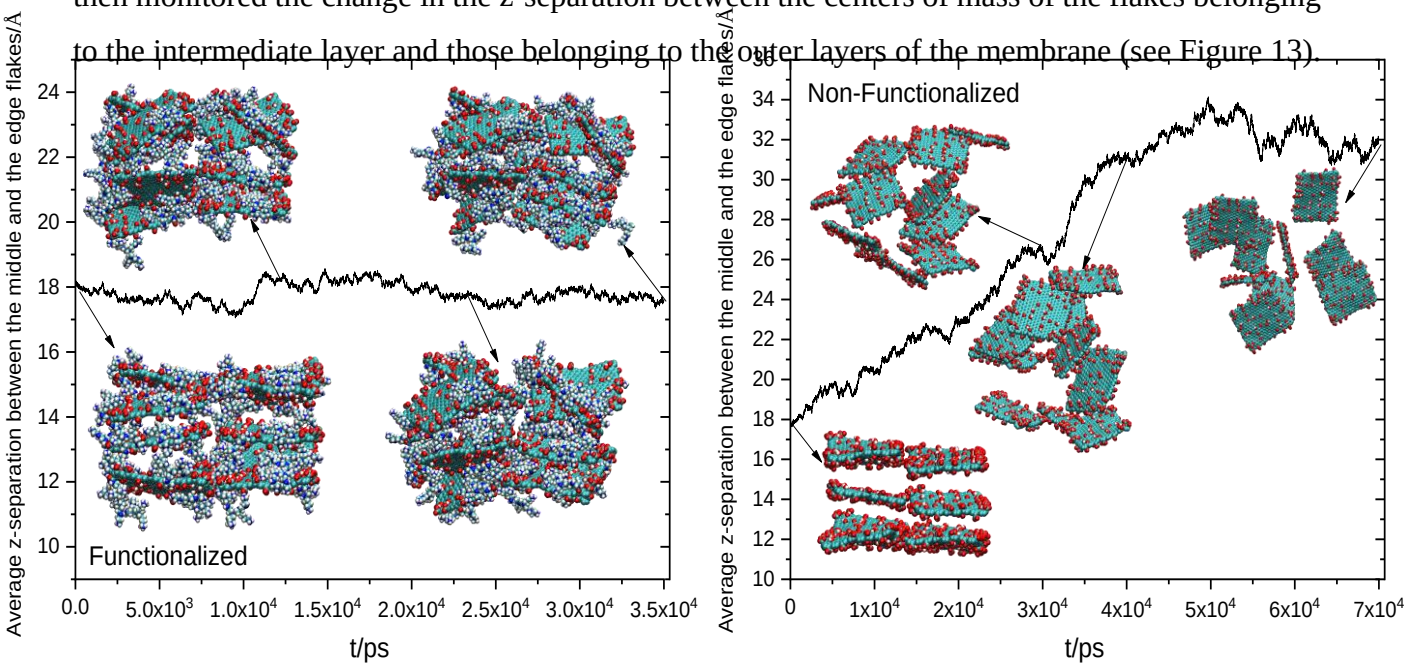

Figure 13: Average z-separation between the flakes of the middle and the outer layers as a function of the time elapsed during an unconstrained simulation. Snapshots of the membrane are shown at different time instants, denoted by the arrows.

The swelling behavior of the two types of membranes is distinctly different. For the non-functionalized system an initial increase in the separation between the layers is observed, which appears to level-off after several tens of ns. For the functionalized model the same measure shows only small fluctuations around the initial value. The behavior exhibited by the non-functionalized flakes, is consistent with the picture described in our previous work[24], where it was shown that depending on the concentration (and in the absence of any supporting surface), these flakes may either disperse or organize in clusters. On the other hand, the functionalized flakes show a trend to remain assembled. The average layer separation is larger compared to the 11.6Å-12.4Å measured for fully hydrated GO membranes[115], providing additional evidence that functionalization is an effective means towards controlling the interlayer spacing of such membranes[72].

The apparent higher affinity between the functionalized flakes, can be associated with their ability to form both, a considerably larger number of hydrogen bonds with water (see figure 8) which acts towards stabilizing the structure, and a larger number (more than double according to our calculation) of inter-flake hydrogen bonds, compared to their non-functionalized counterparts. The lower overall charge per functionalized flake (i.e., +1|e|) facilitates their approach and enhances the probability for hydrogen bond formation by the larger number of donors that they can dispose.

4. Conclusions

In this work we have examined for the first time through fully atomistic NEMD simulations, GO-based multilayered membranes comprised by PEI-functionalized electrically charged flakes and compared their performance in water permeability and salt rejection with analogous non-functionalized models. We explored pressure gradients ranging from levels realizable to actual RO operations, i.e., ~100bar to 10-fold higher values, i.e., ~1000bar. In addition, we explored the effects of imposing different types of motional constraints on the flakes comprising the membranes, including the ability of the flakes to assume a free rotation around their centers of mass.

In all models, a higher degree of motional freedom of the flakes led to an increase in water permeability by approximately 9% for the functionalized and 6% for the non-functionalized ones, while resulting only in minor fluctuations regarding their salt rejection performance. This implies

that the structural flexibility of the membrane does play a role in RO processes, and it should be taken into account when optimization of the operational conditions is attempted.

The presence of the branched PEI attached on GO was associated with a higher degree of hydrogen bonding between the flakes and the water molecules, resulting in a reduction of approximately 30% in water permeability. The presence of the PEI branches resulted in a higher than 20% increase in salt rejection at pressure difference levels close to those in actual RO operations. The salt rejection levels observed at the lowest examined pressure difference was close to 75% for the functionalized models, but this is expected to be mitigated by designing a membrane with more layers. The functionalized membranes did not exhibit any significant levels of selectivity regarding the Na^+ or the Cl^- ions, while the non-functionalized models showed a somewhat higher ion rejection for the negatively charged chlorine ions. This finding might be related to the fact that in the non-functionalized models a significantly higher concentration of neutralizing sodium ions is present within the membrane.

A non-linear dependence of the degree of salt rejection on the applied pressure difference was found for all the examined models. This observation suggests that caution should be exercised when the linear dependence observed at higher pressure differences is attempted to be extrapolated at the relevant to experimental conditions, lower pressures. An increase of the pressure gradient resulted in a moderate increase (with a trend for levelling-off) of the fraction of the rejected ions. This behavior was attributed to the development of CP due to the accumulation of ions in the feed side close to the membrane's boundary.

Simulations in unconstrained membranes under zero pressure difference, indicated a non-swelling behavior and a trend for structural coherence within the timescale of the simulation, for the models comprised by the functionalized flakes. In these membranes, the interlayer separation between the GO flakes which were functionalized with a 2^{nd} generation poly(ethyleneimine) of Mw~600 Da, was determined to be close to 18Å.

Based on the above findings, we believe that this work offers new insights on the relative contribution of different parameters associated with the water permeability and the salt-rejection performance, and it will be useful for optimizing the design of graphene-oxide-based multilayer membranes for desalination purposes.

CRediT authorship contribution statement

KK: Conceptualization, Methodology, Investigation, Software, Formal analysis, Data Curation, Resources, Writing - Original Draft, Visualization, Funding acquisition
GSF: Methodology, Software, Formal analysis, Resources, Writing - Review & Editing
IZ: Investigation, Writing - Review & Editing, Project administration, Funding acquisition.
HAK: Writing - Review & Editing, Project administration.

Declaration of competing interest The authors declare no competing financial interests regarding the work reported in this paper.

Acknowledgements

This research is supported by ASPIRE, the technology program management pillar of Abu Dhabi's Advanced Technology Research Council (ATRC), via the ASPIRE "AARE (ASPIRE Awards for Research Excellence)" and through grant no. AARE20-246 to Ioannis Zuburtikudis of Abu Dhabi University.
This work was supported by a computational time grant by the Greek Research & Technology Network (GRNET) in the National HPC facility – ARIS – under project ID GOFILTRATION.
Use of computational resources of the AUTh High Performance Computing (HPC) infrastructure of the Aristotle University of Thessaloniki is also acknowledged.

References

[1] J.R. Werber, C.O. Osuji, M. Elimelech, Materials for next-generation desalination and water purification membranes, Nat. Rev. Mater. 1(5) (2016) 16018.
[2] S. Homaeigohar, M. Elbahri, Graphene membranes for water desalination, NPG Asia Mater. 9 (2017) e427.
[3] R. Rashid, I. Shafiq, P. Akhter, M.J. Iqbal, M. Hussain, A state-of-the-art review on wastewater treatment techniques: the effectiveness of adsorption method, Environ. Sci. Pollut. Res. 28(8) (2021) 9050-9066.
[4] P. Rajasulochana, V. Preethy, Comparison on efficiency of various techniques in treatment of waste and sewage water – A comprehensive review, Resource-Efficient Technologies 2(4) (2016) 175-184.
[5] N.H. Othman, N.H. Alias, N.S. Fuzil, F. Marpani, M.Z. Shahruddin, C.M. Chew, K.M. David Ng, W.J. Lau, A.F. Ismail, A Review on the Use of Membrane Technology Systems in Developing Countries, Membranes 12(1) (2021) 30.
[6] A. Anand, B. Unnikrishnan, J.-Y. Mao, H.-J. Lin, C.-C. Huang, Graphene-based nanofiltration membranes for improving salt rejection, water flux and antifouling–A review, Desalination 429 (2018) 119-133.
[7] P. Sun, K. Wang, H. Zhu, Recent Developments in Graphene-Based Membranes: Structure, Mass-Transport Mechanism and Potential Applications, Adv. Mater. 28(12) (2016) 2287-2310.
[8] A. Boretti, S. Al-Zubaidy, M. Vaclavikova, M. Al-Abri, S. Castelletto, S. Mikhalovsky, Outlook for graphene-based desalination membranes, npj Clean Water 1(1) (2018) 5.
[9] T. Yang, H. Lin, X. Zheng, K.P. Loh, B. Jia, Tailoring pores in graphene-based materials: from generation to applications, J. Mater. Chem. A 5(32) (2017) 16537-16558.

[10] T. Tene, G. Tubon Usca, M. Guevara, R. Molina, F. Veltri, M. Arias, L.S. Caputi, C. Vacacela Gomez, Toward Large-Scale Production of Oxidized Graphene, Nanomaterials (Basel, Switzerland) 10(2) (2020) 279.
[11] M. Zhang, H. Yan, X. Yang, C. Liu, Effect of functionalized graphene oxide with a hyperbranched cyclotriphosphazene polymer on mechanical and thermal properties of cyanate ester composites, RSC Adv. 4(86) (2014) 45930-45938.
[12] Y. Yu, L.C.X. De Andrade, L.M. Fang, J. Ma, W.J. Zhang, Y.H. Tang, Graphene oxide and hyperbranched polymer-toughened hydrogels with improved absorption properties and durability, J. Mater. Sci. 50(9) (2015) 3457-3466.
[13] P.S. Parsamehr, M. Zahed, M.A. Tofighy, T. Mohammadi, M. Rezakazemi, Preparation of novel cross-linked graphene oxide membrane for desalination applications using (EDC and NHS)-activated graphene oxide and PEI, Desalination 468 (2019) 114079.
[14] Y. Wenzheng, Y. Tong, G. Nigel, Development of a stable cation modified graphene oxide membrane for water treatment, 2D Mater. 4(4) (2017) 045006.
[15] A. Nicolai, B.G. Sumpter, V. Meunier, Tunable water desalination across graphene oxide framework membranes, Phys. Chem. Chem. Phys. 16(18) (2014) 8646-8654.
[16] K.H. Thebo, X. Qian, Q. Zhang, L. Chen, H.-M. Cheng, W. Ren, Highly stable graphene-oxide-based membranes with superior permeability, Nat. Commun. 9(1) (2018) 1486-1486.
[17] A. Ghaffar, L. Zhang, X. Zhu, B. Chen, Scalable graphene oxide membranes with tunable water channels and stability for ion rejection, Environ. Sci. Nano 6(3) (2019) 904-915.
[18] L. Chen, G. Shi, J. Shen, B. Peng, B. Zhang, Y. Wang, F. Bian, J. Wang, D. Li, Z. Qian, G. Xu, G. Liu, J. Zeng, L. Zhang, Y. Yang, G. Zhou, M. Wu, W. Jin, J. Li, H. Fang, Ion sieving in graphene oxide membranes via cationic control of interlayer spacing, Nature 550(7676) (2017) 380-383.
[19] H.B. Park, J. Kamcev, L.M. Robeson, M. Elimelech, B.D. Freeman, Maximizing the right stuff: The trade-off between membrane permeability and selectivity, Science 356(6343) (2017).
[20] A. Alkhouzaam, H. Qiblawey, Functional GO-based membranes for water treatment and desalination: Fabrication methods, performance and advantages. A review, Chemosphere 274 (2021) 129853.
[21] M. Hosseini, J. Azamat, H. Erfan-Niya, Water desalination through fluorine-functionalized nanoporous graphene oxide membranes, Mater. Chem. Phys. 223 (2019) 277-286.
[22] Q. Huang, G. Li, M. Chen, S. Dong, Graphene oxide functionalized O-(carboxymethyl)-chitosan membranes: Fabrication using dialysis and applications in water purification, Colloids Surf. A 554 (2018) 27-33.
[23] A.K. Giri, F. Teixeira, M.N.D.S. Cordeiro, Salt separation from water using graphene oxide nanochannels: A molecular dynamics simulation study, Desalination 460 (2019) 1-14.
[24] A.N. Rissanou, I. Karnis, F. Krasanakis, K. Chrissopoulou, K. Karatasos, The Role of Oxidation Pattern and Water Content in the Spatial Arrangement and Dynamics of Oxidized Graphene-Based Aqueous Dispersions, Int. J. Mol. Sci. 23 (2022) 13459.
[25] B. Chen, H. Jiang, X. Liu, X. Hu, Observation and Analysis of Water Transport through Graphene Oxide Interlamination, J. Phys. Chem. C 121(2) (2017) 1321-1328.
[26] H. Dai, Z. Xu, X. Yang, Water Permeation and Ion Rejection in Layer-by-Layer Stacked Graphene Oxide Nanochannels: A Molecular Dynamics Simulation, J. Phys. Chem. C 120(39) (2016) 22585-22596.
[27] W.D. Xiao, B. Yan, H.B. Zeng, Q.X. Liu, Dendrimer functionalized graphene oxide for selenium removal, Carbon 105 (2016) 655-664.

[28] Q.H. Xu, Y.W. Gong, Y. Fang, G.H. Jiang, Y. Wang, X.K. Sun, R.J. Wang, Straightforward synthesis of hyperbranched polymer/graphene nanocomposites from graphite oxide via in situ grafting from approach, Bull. Mater. Sci. 35(5) (2012) 795-800.
[29] S.M. Shau, T.Y. Juang, H.S. Lin, C.L. Huang, C.F. Hsieh, J.Y. Wu, R.J. Jeng, Individual graphene oxide platelets through direct molecular exfoliation with globular amphiphilic hyperbranched polymers, Polym. Chem. 3(5) (2012) 1249-1259.
[30] A. Rissanou, A. Konstantinou, K. Karatasos, Morphology and Dynamics in Hydrated Graphene Oxide/Branched Poly(ethyleneimine) Nanocomposites: An In Silico Investigation, Nanomaterials 13(12) (2023) 1865.
[31] R.S. DeFever, N.K. Geitner, P. Bhattacharya, F. Ding, P.C. Ke, S. Sarupria, PAMAM Dendrimers and Graphene: Materials for Removing Aromatic Contaminants from Water, Environ. Sci. Technol. 49(7) (2015) 4490-4497.
[32] Z. Sideratou, M. Agathokleous, T.A. Theodossiou, D. Tsiourvas, Functionalized Hyperbranched Polyethylenimines as Thermosensitive Drug Delivery Nanocarriers with Controlled Transition Temperatures, Biomacromolecules 19(2) (2018) 315-328.
[33] E.A. Müller, Purification of water through nanoporous carbon membranes: a molecular simulation viewpoint, Curr. Opin. Chem. Eng. 2(2) (2013) 223-228.
[34] R.K. Joshi, P. Carbone, F.C. Wang, V.G. Kravets, Y. Su, I.V. Grigorieva, H.A. Wu, A.K. Geim, R.R. Nair, Precise and Ultrafast Molecular Sieving Through Graphene Oxide Membranes, Science 343(6172) (2014) 752-754.
[35] D. Konatham, J. Yu, T.A. Ho, A. Striolo, Simulation Insights for Graphene-Based Water Desalination Membranes, Langmuir 29(38) (2013) 11884-11897.
[36] D. Cohen-Tanugi, J.C. Grossman, Water Desalination across Nanoporous Graphene, Nano Lett. 12(7) (2012) 3602-3608.
[37] P. Ansari, J. Azamat, A. Khataee, Separation of perchlorates from aqueous solution using functionalized graphene oxide nanosheets: a computational study, J. Mater. Sci. 54(3) (2019) 2289-2299.
[38] P.S. Goh, T. Matsuura, A.F. Ismail, B.C. Ng, The Water-Energy Nexus: Solutions towards Energy-Efficient Desalination, Energy Technol. 5(8) (2017) 1136-1155.
[39] Y. Han, Z. Xu, C. Gao, Ultrathin Graphene Nanofiltration Membrane for Water Purification, Adv. Funct. Mater. 23(29) (2013) 3693-3700.
[40] K. Huang, G. Liu, Y. Lou, Z. Dong, J. Shen, W. Jin, A Graphene Oxide Membrane with Highly Selective Molecular Separation of Aqueous Organic Solution, Angew. Chem. Int. Ed. 53(27) (2014) 6929-6932.
[41] H. Zarrin, S. Sy, J. Fu, G. Jiang, K. Kang, Y.-S. Jun, A. Yu, M. Fowler, Z. Chen, Molecular Functionalization of Graphene Oxide for Next-Generation Wearable Electronics, ACS Appl. Mater. Interfaces 8(38) (2016) 25428-25437.
[42] P. Sun, M. Zhu, K. Wang, M. Zhong, J. Wei, D. Wu, Z. Xu, H. Zhu, Selective Ion Penetration of Graphene Oxide Membranes, ACS Nano 7(1) (2012) 428-437.
[43] W. Choi, J. Choi, J. Bang, J.-H. Lee, Layer-by-Layer Assembly of Graphene Oxide Nanosheets on Polyamide Membranes for Durable Reverse-Osmosis Applications, ACS Appl. Mater. Interfaces 5(23) (2013) 12510-12519.
[44] M. Hu, B. Mi, Enabling Graphene Oxide Nanosheets as Water Separation Membranes, Environ. Sci. Technol. 47(8) (2013) 3715-3723.
[45] Y. Wei, Y. Zhang, X. Gao, Z. Ma, X. Wang, C. Gao, Multilayered graphene oxide membranes for water treatment: A review, Carbon 139 (2018) 964-981.

[46] N. Wei, X. Peng, Z. Xu, Understanding Water Permeation in Graphene Oxide Membranes, ACS Appl. Mater. Interfaces 6(8) (2014) 5877-5883.
[47] D. Cohen-Tanugi, L.-C. Lin, J.C. Grossman, Multilayer Nanoporous Graphene Membranes for Water Desalination, Nano Lett. 16(2) (2016) 1027-1033.
[48] J.A.L. Willcox, H.J. Kim, Molecular Dynamics Study of Water Flow across Multiple Layers of Pristine, Oxidized, and Mixed Regions of Graphene Oxide, ACS Nano 11(2) (2017) 2187-2193.
[49] S. Safaei, R. Tavakoli, On the design of graphene oxide nanosheets membranes for water desalination, Desalination 422(Supplement C) (2017) 83-90.
[50] M. Shahbabaei, D. Tang, D. Kim, Simulation insight into water transport mechanisms through multilayer graphene-based membrane, Comput. Mater. Sci. 128 (2017) 87-97.
[51] E. Soleimani, M. Foroutan, Multilayer graphene with a rippled structure for water desalination, J. Mol. Liq. 265 (2018) 208-215.
[52] A. Gogoi, K. Anki Reddy, P. Mondal, Multilayer Graphene Oxide Membrane in Forward Osmosis: Molecular Insights, ACS Appl. Nano Mater. 1(9) (2018) 4450-4460.
[53] P. Wang, Y.X. Jia, R. Yan, M. Wang, Graphene oxide proton permselective membrane for electrodialysis-based waste acid reclamation: Simulation and validation, J. Memb. Sci. 640 (2021) 119853.
[54] C. Muzzi, A. Gotzias, E. Fontananova, E. Tocci, Stability of Graphene Oxide Composite Membranes in an Aqueous Environment from a Molecular Point of View, Applied Sciences 12(7) (2022) 3460.
[55] J. Zhang, C. Chen, J. Pan, L. Zhang, L. Liang, Z. Kong, X. Wang, W. Zhang, J.-W. Shen, Atomistic insights into the separation mechanism of multilayer graphene membranes for water desalination, Phys. Chem. Chem. Phys. 22(14) (2020) 7224-7233.
[56] M. Kargar, F. Khashei Varnamkhasti, A. Lohrasebi, Influence of electric fields on the efficiency of multilayer graphene membrane, J. Mol. Model. 24(9) (2018).
[57] M. Akhavan, J. Schofield, S. Jalili, Water transport and desalination through double-layer graphyne membranes, Phys. Chem. Chem. Phys. 20(19) (2018) 13607-13615.
[58] Q. Shi, H. Gao, Y. Zhang, Z. Meng, D. Rao, J. Su, Y. Liu, Y. Wang, R. Lu, Bilayer graphene with ripples for reverse osmosis desalination, Carbon 136 (2018) 21-27.
[59] C. Fritzmann, J. Löwenberg, T. Wintgens, T. Melin, State-of-the-art of reverse osmosis desalination, Desalination 216(1-3) (2007) 1-76.
[60] M. Qasim, M. Badrelzaman, N.N. Darwish, N.A. Darwish, N. Hilal, Reverse osmosis desalination: A state-of-the-art review, Desalination 459 (2019) 59-104.
[61] L. Yan, Y.-N. Chang, L. Zhao, Z. Gu, X. Liu, G. Tian, L. Zhou, W. Ren, S. Jin, W. Yin, H. Chang, G. Xing, X. Gao, Y. Zhao, The use of polyethylenimine-modified graphene oxide as a nanocarrier for transferring hydrophobic nanocrystals into water to produce water-dispersible hybrids for use in drug delivery, Carbon 57 (2013) 120-129.
[62] E. Halakoo, X. Feng, Layer-by-layer assembly of polyethyleneimine/graphene oxide membranes for desalination of high-salinity water via pervaporation, Sep. Purif. Technol. 234 (2020) 116077.
[63] F. Arshad, M. Selvaraj, J. Zain, F. Banat, M.A. Haija, Polyethylenimine modified graphene oxide hydrogel composite as an efficient adsorbent for heavy metal ions, Sep. Purif. Technol. 209 (2019) 870-880.

[64] H. Ahmad, C. Cai, C. Liu, Separation and preconcentration of Pb(II) and Cd(II) from aqueous samples using hyperbranched polyethyleneimine-functionalized graphene oxide-immobilized polystyrene spherical adsorbents, Microchem. J. 145 (2019) 833-842.
[65] Q. Zhao, X. Zhu, B. Chen, Stable graphene oxide/poly(ethyleneimine) 3D aerogel with tunable surface charge for high performance selective removal of ionic dyes from water, Chem. Eng. J. 334 (2018) 1119-1127.
[66] H. Ahmad, K. Umar, S.G. Ali, P. Singh, S.S. Islam, H.M. Khan, Preconcentration and speciation of arsenic by using a graphene oxide nanoconstruct functionalized with a hyperbranched polyethyleneimine, Mikrochim Acta 185(6) (2018) 290.
[67] X. Wang, Q. Liu, J. Liu, R. Chen, H. Zhang, R. Li, Z. Li, J. Wang, 3D self-assembly polyethyleneimine modified graphene oxide hydrogel for the extraction of uranium from aqueous solution, Appl. Surf. Sci. 426 (2017) 1063-1074.
[68] I. Tanis, E. Kostarellou, K. Karatasos, Molecular dynamics simulations of hyperbranched poly(ethylene imine)-graphene oxide nanocomposites as dye adsorbents for water purification, Phys. Chem. Chem. Phys. 23(40) (2021) 22874-22884.
[69] A. Lerf, H. He, M. Forster, J. Klinowski, Structure of Graphite Oxide Revisited, J. Phys. Chem. B . 102(23) (1998) 4477-4482.
[70] B. Konkena, S. Vasudevan, Understanding Aqueous Dispersibility of Graphene Oxide and Reduced Graphene Oxide through pKa Measurements, J. Phys. Chem. Lett. 3(7) (2012) 867-872.
[71] Y. Zhang, S. Zhang, T.-S. Chung, Nanometric Graphene Oxide Framework Membranes with Enhanced Heavy Metal Removal via Nanofiltration, Environ. Sci. Technol. 49(16) (2015) 10235-10242.
[72] J.-J. Lu, Y.-H. Gu, Y. Chen, X. Yan, Y.-J. Guo, W.-Z. Lang, Ultrahigh permeability of graphene-based membranes by adjusting D-spacing with poly (ethylene imine) for the separation of dye wastewater, Sep. Purif. Technol. 210 (2019) 737-745.
[73] F. Morales-Lara, M. Domingo-García, R. López-Garzón, M. Luz Godino-Salido, A. Peñas-Sanjuán, F.J. López-Garzón, M. Pérez-Mendoza, M. Melguizo, Grafting the surface of carbon nanotubes and carbon black with the chemical properties of hyperbranched polyamines, Sci Technol Adv Mater. 17(1) (2016) 541-553.
[74] Y.G. Yan, W.S. Wang, W. Li, K.P. Loh, J. Zhang, A graphene-like membrane with an ultrahigh water flux for desalination, Nanoscale 9(47) (2017) 18951-18958.
[75] J. Wang, P. Zhang, B. Liang, Y. Liu, T. Xu, L. Wang, B. Cao, K. Pan, Graphene Oxide as an Effective Barrier on a Porous Nanofibrous Membrane for Water Treatment, ACS Appl. Mater. Interfaces 8(9) (2016) 6211-6218.
[76] J. Ding, H. Zhao, B. Xu, H. Yu, Biomimetic Sustainable Graphene Ultrafast-Selective Nanofiltration Membranes, ACS Sustain. Chem. Eng. 8(24) (2020) 8986-8993.
[77] T. Chen, F.S. Butt, M. Zhang, X. Wei, A. Lewis, N. Radacsi, A.J.C. Semiao, J. Han, Y. Huang, Ultra-permeable zeolitic imidazolate frameworks-intercalated graphene oxide membranes for unprecedented ultrafast molecular separation, Chem. Eng. J. 419 (2021) 129507.
[78] F.J. Millero, R. Feistel, D.G. Wright, T.J. McDougall, The composition of Standard Seawater and the definition of the Reference-Composition Salinity Scale, Deep Sea Res. Part I Oceanogr. Res. Pap. 55(1) (2008) 50-72.
[79] L. Gazagnes, S. Cerneaux, M. Persin, E. Prouzet, A. Larbot, Desalination of sodium chloride solutions and seawater with hydrophobic ceramic membranes, Desalination 217(1) (2007) 260-266.

[80] M. Heiranian, A.B. Farimani, N.R. Aluru, Water desalination with a single-layer MoS2 nanopore, Nat. Commun. 6 (2015) 8616-8616.
[81] W.L. Jorgensen, D.S. Maxwell, J. Tirado-Rives, Development and Testing of the OPLS All-Atom Force Field on Conformational Energetics and Properties of Organic Liquids, J. Am. Chem. Soc. 118(45) (1996) 11225-11236.
[82] H. Tang, Y. Zhao, X.N. Yang, D.M. Liu, S.J. Shan, F.Y. Cui, B.S. Xing, Understanding the pH-dependent adsorption of ionizable compounds on graphene oxide using molecular dynamics simulations, Environ. Sci. Nano 4(10) (2017) 1935-1943.
[83] Y. Ai, Y. Liu, Y. Huo, C. Zhao, L. Sun, B. Han, X. Cao, X. Wang, Insights into the adsorption mechanism and dynamic behavior of tetracycline antibiotics on reduced graphene oxide (RGO) and graphene oxide (GO) materials, Environ. Sci. Nano 6(11) (2019) 3336-3348.
[84] H. Tang, Y. Zhao, X.N. Yang, D.M. Liu, P.H. Shao, Z.G. Zhu, S.J. Shan, F.Y. Cui, B.S. Xing, New Insight into the Aggregation of Graphene Oxide Using Molecular Dynamics Simulations and Extended Derjaguin-Landau-Verwey-Overbeek Theory, Environ. Sci. Technol. 51(17) (2017) 9674-9682.
[85] S. Zheng, Q. Tu, J.J. Urban, S. Li, B. Mi, Swelling of Graphene Oxide Membranes in Aqueous Solution: Characterization of Interlayer Spacing and Insight into Water Transport Mechanisms, ACS Nano 11(6) (2017) 6440-6450.
[86] C. Wu, pH response of conformation of poly(propylene imine) dendrimer in water: a molecular simulation study, Mol. Simulat. 36(14) (2010) 1164-1172.
[87] E. Lin, X. You, R.M. Kriegel, R.D. Moffitt, R.C. Batra, Binding affinity between small molecules in solvent and polymer film using molecular dynamics simulations, Colloid. Surface. A 522 (2017) 152-160.
[88] K.P. Jensen, W.L. Jorgensen, Halide, Ammonium, and Alkali Metal Ion Parameters for Modeling Aqueous Solutions, J. Chem. Theory Comput. 2(6) (2006) 1499-1509.
[89] W.L. Jorgensen, J. Chandrasekhar, J.D. Madura, R.W. Impey, M.L. Klein, Comparison of simple potential functions for simulating liquid water, J. Chem. Phys. 79(2) (1983) 926-935.
[90] M.F. Harrach, B. Drossel, Structure and dynamics of TIP3P, TIP4P, and TIP5P water near smooth and atomistic walls of different hydroaffinity, J. Chem. Phys. 140(17) (2014) 174501.
[91] L. Martínez, R. Andrade, E.G. Birgin, J.M. Martínez, PACKMOL: A package for building initial configurations for molecular dynamics simulations, J. Comput. Chem. 30(13) (2009) 2157-2164.
[92] W. Humphrey, A. Dalke, K. Schulten, VMD: Visual molecular dynamics, J. Mol. Graph. 14(1) (1996) 33-38.
[93] J.C. Phillips, R. Braun, W. Wang, J. Gumbart, E. Tajkhorshid, E. Villa, C. Chipot, R.D. Skeel, L. Kalé, K. Schulten, Scalable molecular dynamics with NAMD, J. Comput. Chem. 26(16) (2005) 1781-1802.
[94] T. Darden, L. Perera, L. Li, L. Pedersen, New tricks for modelers from the crystallography toolkit: the particle mesh Ewald algorithm and its use in nucleic acid simulations, Structure 7(3) (1999) R55-R60.
[95] S.E. Feller, Y. Zhang, R.W. Pastor, B.R. Brooks, Constant pressure molecular dynamics simulation: The Langevin piston method, J. Chem. Phys. 103(11) (1995) 4613-4621.
[96] M. Shen, S. Keten, R.M. Lueptow, Dynamics of water and solute transport in polymeric reverse osmosis membranes via molecular dynamics simulations, J. Memb. Sci. 506 (2016) 95-108.

[97] B. Wu, N. Zhang, M. Zhang, S. Wang, X. Song, Y. Zhou, S. Qi, C. Gao, Towards a High Rejection Desalination Membrane: The Confined Growth of Polyamide Nanofilm Induced by Alkyl-Capped Graphene Oxide, Membranes (Basel) 11(7) (2021) 488.
[98] J. Fuchsberger, P. Aigner, S. Niederer, G. Plank, H. Schima, G. Haase, E. Karabelas, On the incorporation of obstacles in a fluid flow problem using a Navier–Stokes–Brinkman penalization approach, J. Comput. Sci. 57 (2022) 101506.
[99] E.Y.M. Ang, T.Y. Ng, J. Yeo, Z. Liu, K.R. Geethalakshmi, Free-standing graphene slit membrane for enhanced desalination, Carbon 110 (2016) 350-355.
[100] D. Chandler, Introduction to Modern Statistical Mechanics. , Oxford University Press, USA.1987
[101] R. Devanathan, D. Chase-Woods, Y. Shin, D.W. Gotthold, Molecular Dynamics Simulations Reveal that Water Diffusion between Graphene Oxide Layers is Slow, Sci. Rep. 6 (2016) 29484.
[102] P.V. Kumar, M. Bernardi, J.C. Grossman, The Impact of Functionalization on the Stability, Work Function, and Photoluminescence of Reduced Graphene Oxide, ACS Nano 7(2) (2013) 1638-1645.
[103] A.J.P. Neto, V.V. Chaban, E.E. Fileti, Hydration peculiarities of graphene oxides with multiple oxidation degrees, Phys. Chem. Chem. Phys. 19(48) (2017) 32333-32340.
[104] A. Luzar, D. Chandler, Hydrogen-bond kinetics in liquid water, Nature 379(6560) (1996) 55-57.
[105] X. Zhang, M. Wei, F. Xu, Y. Wang, Pressure-Dependent Ion Rejection in Nanopores, J. Phys. Chem. C 124(37) (2020) 20498-20505.
[106] J. Kou, X. Zhou, H. Lu, F. Wu, J. Fan, Graphyne as the membrane for water desalination, Nanoscale 6(3) (2014) 1865-1870.
[107] S. Sarkar, A.K. SenGupta, P. Prakash, The Donnan Membrane Principle: Opportunities for Sustainable Engineered Processes and Materials, Environ. Sci. Technol. 44(4) (2010) 1161-1166.
[108] A.E. Yaroshchuk, Dielectric exclusion of ions from membranes, Adv. Colloid Interface Sci. 85(2) (2000) 193-230.
[109] L. Wang, T. Cao, J.E. Dykstra, S. Porada, P.M. Biesheuvel, M. Elimelech, Salt and Water Transport in Reverse Osmosis Membranes: Beyond the Solution-Diffusion Model, Environ. Sci. Technol. 55(24) (2021) 16665-16675.
[110] K.J. Kim, A.G. Fane, R. Ben Aim, M.G. Liu, G. Jonsson, I.C. Tessaro, A.P. Broek, D. Bargeman, A comparative study of techniques used for porous membrane characterization: pore characterization, J. Memb. Sci. 87(1-2) (1994) 35-46.
[111] E.-S. Jang, W. Mickols, R. Sujanani, A. Helenic, T.J. Dilenschneider, J. Kamcev, D.R. Paul, B.D. Freeman, Influence of concentration polarization and thermodynamic non-ideality on salt transport in reverse osmosis membranes, J. Memb. Sci. 572 (2019) 668-675.
[112] Q.F. Alsalhy, T.M. Albyati, M.A. Zablouk, A study of the effect of operating conditions on reverse osmosis membrane performance with and without air sparging technique, Chem. Eng. Commun. 200(1) (2013) 1-19.
[113] I. Sutzkover, D. Hasson, R. Semiat, Simple technique for measuring the concentration polarization level in a reverse osmosis system, Desalination 131(1) (2000) 117-127.
[114] E.M. Van Wagner, A.C. Sagle, M.M. Sharma, B.D. Freeman, Effect of crossflow testing conditions, including feed pH and continuous feed filtration, on commercial reverse osmosis membrane performance, J. Memb. Sci. 345(1-2) (2009) 97-109.

[115] A. Iakunkov, A.V. Talyzin, Swelling properties of graphite oxides and graphene oxide multilayered materials, Nanoscale 12(41) (2020) 21060-21093.